Scanning Microscopy for Nanotechnology

Scanning Microscopy for Nanotechnology

Techniques and Applications

edited by

Weilie Zhou

University of New Orleans
New Orleans, Louisiana

and

Zhong Lin Wang

Georgia Institute of Technology
Atlanta, Georgia

Weilie Zhou
College of Sciences
University of New Orleans
New Orleans, Louisiana 70148

Zhong Lin Wang
Center of Nanotechnology and
Nanoscience
Georgia Institute of Technology
Atlanta, Georgia 30332

Library of Congress Control Number: 2006925865

ISBN-10: 0-387-33325-8
ISBN-13: 978-0-387-33325-0
e-ISBN-10: 0-387-39620-9
e-ISBN-13: 978-0387-39620-0

Printed on acid-free paper.

© 2006 Springer Science+Business Media, LLC
All rights reserved. This work may not be translated or copied in whole or in part without the written permission of the publisher (Springer Science+Business Media, LLC, 233 Spring Street, New York, NY 10013, USA), except for brief excerpts in connection with reviews or scholarly analysis. Use in connection with any form of information storage and retrieval, electronic adaptation, computer software, or by similar or dissimilar methodology now known or hereafter developed is forbidden.
The use in this publication of trade names, trademarks, service marks, and similar terms, even if they are not identified as such, is not to be taken as an expression of opinion as to whether or not they are subject to proprietary rights.

9 8 7 6 5 4 3 2 1

springer.com

Contributors

Robert Anderhalt
Ametek EDAX Inc.
91 McKee Drive,
Mahwah, NJ 07430

Anzalone, Paul
FEI
5350 NE Dawson Creek Drive
Hillsboro, OR
97124-5793

P. Robert Apkarian
Integrated Microscopy and Microanalytical Facility
Department of Chemistry
Emory University
1521 Dickey Drive
Atlanta GA 30322

A. Borisevich
Oak Ridge National Laboratory
P.O. Box 2008
Oak Ridge, TN 37831

Daniela Caruntu
Advanced Materials Research Institute
University of New Orleans
New Orleans, LA 70148

Gabriel Caruntu
Advanced Materials Research Institute
University of New Orleans
New Orleans, LA 70148

M.F. Chisholm
Oak Ridge National Laboratory
P.O. Box 2008
Oak Ridge, TN 37831

Lesley Anglin Compbell
Advanced Materials Research Institute
University of New Orleans
New Orleans, LA 70148

M. David Frey
Carl Zeiss SMT Inc.
1 Zeiss Drive
Thornwood, NY 10594

Pu Xian Ga
School of Materials Science and Engineering, Georgia Institute of Technology
Atlanta, GA 30332-0245

A. Lucille Giannuzzi
FEI
5350 NE Dawson Creek Drive
Hillsboro, OR
97124-5793

Rishi Gupta
Zyvex
1321 North Plano Road
Richardson, Texas 75081

David Joy
University of Tennessee
Knoxville, TN 37996

Jianye Li
Department of Chemistry
Duke University
Durham, NC 27708-0354

Feng Li
Advanced Materials Research Institute
University of New Orleans
New Orleans, LA 70148

Jie Liu
Department of Chemistry
Duke University
Durham, NC 27708-0354

Xiaohua Liu
Department of Biologic and Materials Sciences
Division of Prosthodontics
University of Michigan
1011 N. University
Ann Arbor, MI 48109-1078

A.R. Lupini
Oak Ridge National Laboratory
P.O. Box 2008
Oak Ridge, TN 37831

Peter X. Ma
Department of Biologic and Materials Sciences
Division of Prosthodontics
University of Michigan
1011 N. University
Ann Arbor, MI 48109-1078

Tim Maitland
HKL Technology Inc
52A Federal Road, Unit 2D
Danbury, CT 06810

Joe Nabity
JC Nabity Lithography Systems
Bozeman, MT 59717

Charles J. O'Connor
Advanced Materials Research Institute
University of New Orleans
New Orleans, LA 70148

M.P. Oxley
Oak Ridge National Laboratory
P.O. Box 2008
Oak Ridge, TN 37831

Y. Peng
Oak Ridge National Laboratory
P.O. Box 2008
Oak Ridge, TN 37831

Steve Pennycook
Oak Ridge National Laboratory
P.O. Box 2008
Oak Ridge, TN 37831

Richard E. Stallcup II
Zyvex
1321 North Plano Road
Richardson, Texas 75081

Scott Sitzman
HKL Technology Inc
52A Federal Road, Unit 2D
Danbury, CT 06810

K. Van Benthem
Oak Ridge National Laboratory
P.O. Box 2008
Oak Ridge, TN 37831

Brandon Van Leer
FEI
5350 NE Dawson Creek Drive
Hillsboro, OR
97124-5793

M. Varela
Oak Ridge National Laboratory
P.O. Box 2008
Oak Ridge, TN 37831

Peng Wang
Department of Biologic and Materials Sciences
Division of Prosthodontics
University of Michigan
1011 N. University
Ann Arbor, MI 48109-1078

Xudong Wang
Center for Nanoscience and Nanotechnology (CNN)
Georgia Institute of Technology
Materials Science and Engineering Department
771 Ferst Drive, N.W.
Atlanta, GA 30332-0245

Zhong Lin Wang
Center for Nanoscience and Nanotechnology
Georgia Institute of Technology
Materials Science and Engineering
771 Ferst Drive, N.W.
Atlanta, GA 30332-0245

Guobao Wei
Department of Biologic and Materials Sciences
Division of Prosthodontics
University of Michigan
1011 N. University
Ann Arbor, MI 48109-1078

John B. Wiley
Department of Chemistry and Advanced Materials Research Institute
University of New Orleans
New Orleans, LA 70148

Weilie Zhou
Advanced Materials Research Institute
University of New Orleans
New Orleans, LA 70148

Mo Zhu
Advanced Materials Research Institute
University of New Orleans
New Orleans, LA 70148

Preface

Advances in nanotechnology over the past decade have made scanning electron microscopy (SEM) an indispensable and powerful tool for analyzing and constructing new nanomaterials. Development of nanomaterials requires advanced techniques and skills to attain higher quality images, understand nanostructures, and improve synthesis strategies. A number of advancements in SEM such as field emission guns, electron back scatter detection (EBSD), and X-ray element mapping have improved nanomaterials analysis. In addition to materials characterization, SEM can be integrated with the latest technology to perform *in-situ* nanomaterial engineering and fabrication. Some examples of this integrated technology include nanomanipulation, electron beam nanolithography, and focused ion beam (FIB) techniques. Although these techniques are still being developed, they are widely applied in every aspect of nanomaterial research. *Scanning Microscopy for Nanotechnology* introduces some of the new advancements in SEM techniques and demonstrate their possible applications.

The first section covers basic theory, newly developed EBSD techniques, advanced X-ray analysis, low voltage imaging, environmental microscopy for biomaterials observation, e-beam nanolithography patterning, FIB nanostructure fabrication, and scanning transmission electron microscopy (STEM). These chapters contain practical examples of how these techniques are used to characterize and fabricate nanomaterials and nanostructures.

The second section discusses the applications of these SEM-based techniques, including nanowires and carbon nanotubes, photonic crystals and devices, nanoparticles and colloidal self-assembly, nano-building blocks fabricated through templates, one-dimensional wurtzite semiconducting nanostructures, bio-inspired nanomaterials, *in-situ* nanomanipulation, and cry-SEM stage in nanostructure research. These applications are widely used in fabricating and engineering new nanomaterials and nanostructures.

A unique feature of this book is that it is written by experts from leading research groups who specialize in the development of nanomaterials using these SEM-based techniques. Additional contributions are made by application specialists from several popular instrument vendors concerning their techniques to

characterize, engineer, and manipulate nanomaterials *in-situ* SEM. *Scanning Microscopy for Nanotechnology* should be a useful and practical guide for nanomaterial researchers as well as a valuable reference book for students and SEM specialists.

Weilie Zhou
Zhong Lin Wang

Contents

1. Fundamentals of Scanning Electron Microscopy (SEM) 1
Weilie Zhou, Robert Apkarian, Zhong Lin Wang, and David Joy

1. Introduction 1
2. Configuration of Scanning Electron Microscopes 9
3. Sample Preparation 32
4. Summary 39

2. Backscattering Detector and EBSD in Nanomaterials Characterization 41
Tim Maitland and Scott Sitzman

1. Introduction 41
2. Data Measurement 51
3. Data Analysis 54
4. Applications 61
5. Current Limitations and Future 74
6. Conclusion 75

3. X-ray Microanalysis in Nanomaterials 76
Robert Anderhalt

1. Introduction 76
2. Monte Carlo Modeling of Nanomaterials 87
3. Case Studies 91
4. Summary 100

4. Low kV Scanning Electron Microscopy 101
M. David Frey

1. Introduction 101
2. Electron Generation and Accelerating Voltage 103
3. "Why Use Low kV?" 105
4. Using Low kV 112
5. Conclusion 119

5. E-beam Nanolithography Integrated with Scanning Electron Microscope 120
Joe Nabity, Lesely Anglin Compbell, Mo Zhu, and Weilie Zhou

1. Introduction 120
2. Materials and Processing Preparation 127
3. Pattern Generation 132
4. Pattern Processing 137
5. Applications 143
6. Summary 148

6. Scanning Transmission Electron Microscopy for Nanostructure Characterization 152
S. J. Pennycook, A. R. Lupini, M. Varela, A. Borisevich, Y. Peng, M. P. Oxley, K. Van Benthem, M. F. Chisholm

1. Introduction 152
2. Imaging in the STEM 155
3. Spectroscopic Imaging 173
4. Three-Dimensional Imaging 176
5. Recent Applications to Nanostructure Characterization 177
6. Future Directions 188

7. Introduction to In-Situ Nanomanipulation for Nanomaterials Engineering 192
Rishi Gupta and Richard E. Stallcup, II

1. Introduction 192
2. SEM Contamination 193
3. Types of Nanomanipulators 197
4. End Effectors 200
5. Applications of Nanomanipulators 205
6. Summary 223

8. Applications of FIB and DualBeam for Nanofabrication 225
Brandon Van Leer, Lucille A. Giannuzzi, and Paul Anzalone

1. Introduction 225
2. Onboard Digital Patterning with the Ion Beam 226
3. FIB Milling or CVD Deposition with Bitmap Files 230
4. Onboard Digital Patterning with the Electron Beam 231
5. Automation for Nanometer Control 233
6. Direct Fabrication of Nanoscale Structures 234
7. Summary 234

9. Nanowires and Carbon Nanotubes 237
Jianye Li and Jie Liu

1. Introduction 237
2. III-V Compound Semiconductors Nanowires 237
3. II-VI Compound Semiconductors Nanowires 250
4. Elemental Nanowires 260
5. Carbon Nanotubes 267
6. Conclusions 278

10. Photonic Crystals and Devices 281
Xudong Wang and Zhong Lin Wang

1. Introduction 281
2. SEM Imaging of Photonic Crystals 289
3. Fabrication of Photonic Crystals in SEM 298
4. Summary 302

11. Nanoparticles and Colloidal Self-assembly 306
Gabriel Caruntu, Daniela Caruntu, and Charles J. O'Connor

1. Introduction 306
2. Metal Nanoparticles 307
3. Mesoporous and Nanoporous Metal Nanostructures 322
4. Nanocrystalline Oxide 329
5. Nanostructured Semiconductor and Thermoelectric Materials . . . 347
6. Conclusions 353

12. Nano-building Blocks Fabricated through Templates 357
Feng Li and John B. Wiley

1. Introduction 357
2. Materials and Methods 358
3. Nano-Building Blocks 361
4. Conclusions 380

13. One-dimensional Wurtzite Semiconducting Nanostructures 384
Pu Xian Gao and Zhong Lin Wang

1. Introduction 384
2. Synthesis and Fabrication of 1D Nanostructures 384
3. One-Dimensional Metal Oxide Nanostructures 389
4. Growth Mechanisms 414
5. Summary 423

14. Bio-inspired Nanomaterials 427
Peng Wang, Guobao Wei, Xiaohua Liu, and Peter X. Ma

1. Introduction 427
2. Nanofibers 429
3. Nanoparticles 444
4. Surface Modification 455
5. Summary 462

15. Cryo-Temperature Stages in Nanostructural Research 467
Robert P. Apkarian

1. Introduction 467
2. Terminology Used in Cryo-HRSEM of Aqueous Systems 468
3. Liquid Water, Ice, and Vitrified Water 469
4. History of Low Temperature SEM 472
5. Instrumentation and Methods 473

Author Index 491

Subject Index 513

1
Fundamentals of Scanning Electron Microscopy

Weilie Zhou, Robert P. Apkarian, Zhong Lin Wang, and David Joy

1. Introduction

The scanning electron microscope (SEM) is one of the most versatile instruments available for the examination and analysis of the microstructure morphology and chemical composition characterizations. It is necessary to know the basic principles of light optics in order to understand the fundamentals of electron microscopy. The unaided eye can discriminate objects subtending about 1/60° visual angle, corresponding to a resolution of ~0.1 mm (at the optimum viewing distance of 25 cm). Optical microscopy has the limit of resolution of ~2,000 Å by enlarging the visual angle through optical lens. Light microscopy has been, and continues to be, of great importance to scientific research. Since the discovery that electrons can be deflected by the magnetic field in numerous experiments in the 1890s [1], electron microscopy has been developed by replacing the light source with high-energy electron beam. In this section, we will, for a split second, go over the theoretical basics of scanning electron microscopy including the resolution limitation, electron beam interactions with specimens, and signal generation.

1.1. Resolution and Abbe's Equation

The limit of resolution is defined as the minimum distances by which two structures can be separated and still appear as two distinct objects. Ernst Abbe [1] proved that the limit of resolution depends on the wavelength of the illumination source. At certain wavelength, when resolution exceeds the limit, the magnified image blurs.

Because of diffraction and interference, a point of light cannot be focused as a perfect dot. Instead, the image will have the appearance of a larger diameter than the source, consisting of a disk composed of concentric circles with diminishing intensity. This is known as an Airy disk and is represented in Fig. 1.1a. The primary wave front contains approximately 84% of the light energy, and the intensity of secondary and tertiary wave fronts decay rapidly at higher orders. Generally, the radius of Airy disk is defined as the distance between the first-order peak and

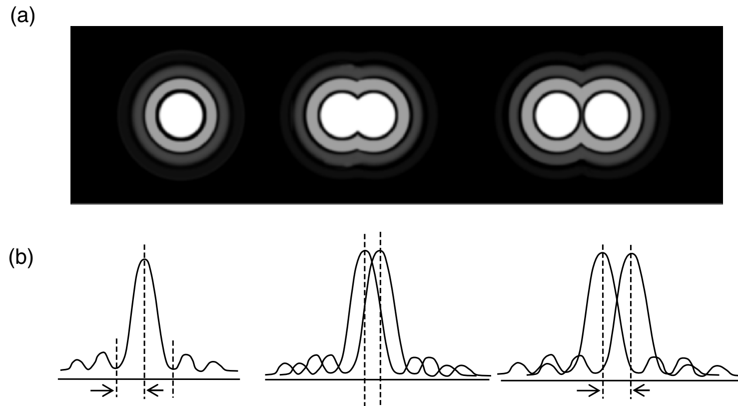

FIGURE 1.1. Illustration of resolution in (a) Airy disk and (b) wave front.

the first-order trough, as shown in Fig. 1.1a. When the center of two primary peaks are separated by a distance equal to the radius of Airy disk, the two objects can be distinguished from each other, as shown in Fig. 1.1b. Resolution in a perfect optical system can be described mathematically by Abbe's equation. In this equation:

$$d = 0.612\ \lambda / n \sin \alpha$$

where
d = resolution
λ = wavelength of imaging radiation
n = index of refraction of medium between point source and lens, relative to free space
α = half the angle of the cone of light from specimen plane accepted by the objective (half aperture angle in radians)
$n \sin \alpha$ is often called numerical aperture (NA).

Substituting the illumination source and condenser lens with electron beam and electromagnetic coils in light microscopes, respectively, the first transmission electron microscope (TEM) was constructed in the 1930s [2], in which electron beam was focused by an electromagnetic condenser lens onto the specimen plane. The SEM utilizes a focused electron beam to scan across the surface of the specimen systematically, producing large numbers of signals, which will be discussed in detail later. These electron signals are eventually converted to a visual signal displayed on a cathode ray tube (CRT).

1.1.1. Interaction of Electron with Samples

Image formation in the SEM is dependent on the acquisition of signals produced from the electron beam and specimen interactions. These interactions can be divided into two major categories: elastic interactions and inelastic interactions.

Elastic scattering results from the deflection of the incident electron by the specimen atomic nucleus or by outer shell electrons of similar energy. This kind of interaction is characterized by negligible energy loss during the collision and by a wide-angle directional change of the scattered electron. Incident electrons that are elastically scattered through an angle of more than 90° are called backscattered electrons (BSE), and yield a useful signal for imaging the sample. Inelastic scattering occurs through a variety of interactions between the incident electrons and the electrons and atoms of the sample, and results in the primary beam electron transferring substantial energy to that atom. The amount of energy loss depends on whether the specimen electrons are excited singly or collectively and on the binding energy of the electron to the atom. As a result, the excitation of the specimen electrons during the ionization of specimen atoms leads to the generation of secondary electrons (SE), which are conventionally defined as possessing energies of less than 50 eV and can be used to image or analyze the sample. In addition to those signals that are utilized to form an image, a number of other signals are produced when an electron beam strikes a sample, including the emission of characteristic x-rays, Auger electrons, and cathodoluminescence. We will discuss these signals in the later sections. Figure 1.2 shows the regions from which different signals are detected.

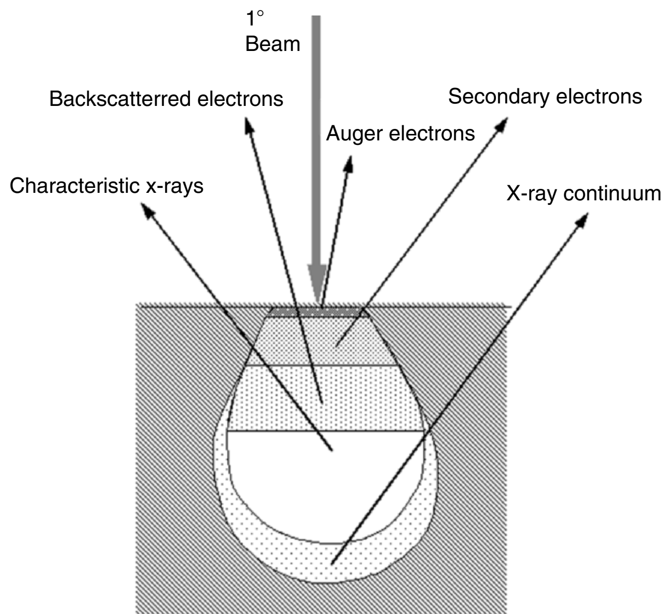

FIGURE 1.2. Illustration of several signals generated by the electron beam–specimen interaction in the scanning electron microscope and the regions from which the signals can be detected.

In most cases when incident electron strikes the specimen surface, instead of being bounced off immediately, the energetic electrons penetrate into the sample for some distance before they encounter and collide with a specimen atom. In doing so, the primary electron beam produces what is known as a region of primary excitation, from which a variety of signals are produced. The size and shape of this zone is largely dependent upon the beam electron energy and the atomic number, and hence the density, of the specimen. Figure 1.3 illustrates the variation of interaction volume with respect to different accelerating voltage and atomic number. At certain accelerating voltage, the shape of interaction volume is "tear drop" for low atomic number specimen and hemisphere for specimens of high atomic number. The volume and depth of penetration increase with an increase of the beam energy and fall with the increasing specimen atomic number because specimens with higher atomic number have more particles to stop electron penetration. One influence of the interaction volume on signal acquisition is that use of a high accelerating voltage will result in deep penetration length and a large primary excitation region, and ultimately cause the loss of detailed surface information of the samples. A close-packed opal structure observed by a field emission scanning electron microscope (FESEM) at different accelerating voltages is shown in Fig. 1.4. Images taken under 1 kV gave more surface details than that of 20 kV. The surface resolution is lost at high accelerating voltages and the surface of spheres looks smooth.

1.1.2. Secondary Electrons

The most widely used signal produced by the interaction of the primary electron beam with the specimen is the secondary electron emission signal. When the primary beam strikes the sample surface causing the ionization of specimen atoms,

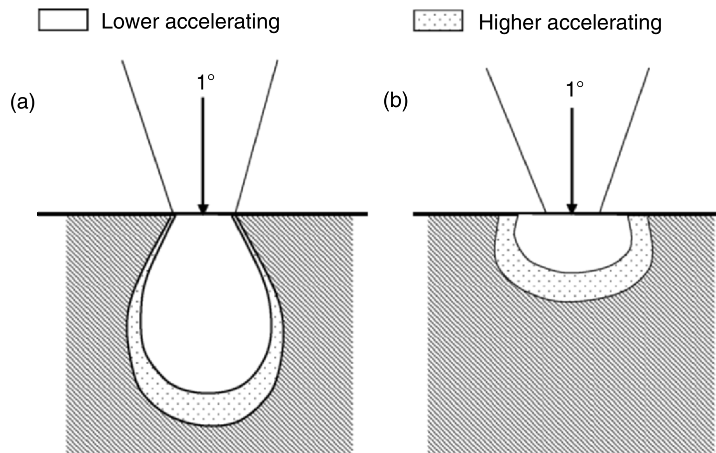

FIGURE 1.3. Influence of accelerating voltage and specimen atomic number on the primary excitation volume: (a) low atomic number and (b) high atomic number.

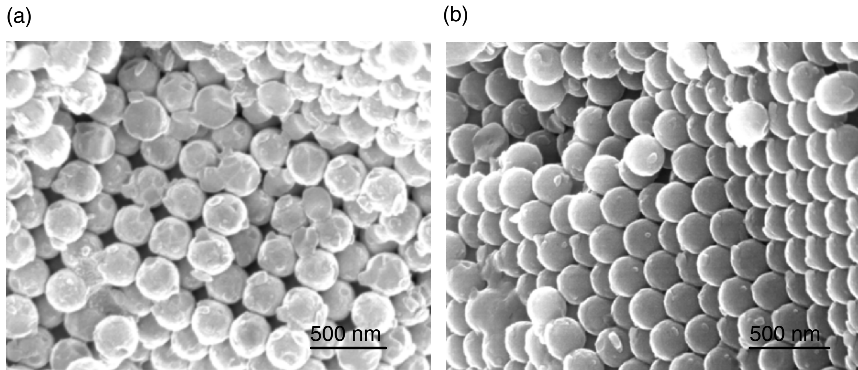

FIGURE 1.4. Scanning electron micrographs of a CaF_2 close-packed opal structure, which are taken under different accelerating voltages: (a) 1 kV and (b) 20 kV.

loosely bound electrons may be emitted and these are referred to as secondary electrons. As they have low energy, typically an average of around 3–5 eV, they can only escape from a region within a few nanometers of the material surface. So secondary electrons accurately mark the position of the beam and give topographic information with good resolution. Because of their low energy, secondary electrons are readily attracted to a detector carrying some applied bias. The Everhart–Thornley (ET) detector, which is the standard collector for secondary electrons in most SEMs therefore applies both a bias (+10 kV) to the scintillator and a lower bias (+300 V) to the Faraday cage, which screens the detector. In order to detect the secondary electrons a scintillator converts the energy of the electrons into photons (visible light). The photons then produced travel down a Plexiglas or polished quartz light pipe and move out through the specimen chamber wall, and into a photomultiplier tube (PMT) which converts the quantum energy of the photons back into electrons. The output voltage from the PMT is further amplified before being output as brightness modulation on the display screen of the SEM.

Secondary electrons are used principally for topographic contrast in the SEM, i.e., for the visualization of surface texture and roughness. The topographical image is dependent on how many of the secondary electrons actually reach the detector. A secondary electron signal can resolve surface structures down to the order of 10 nm or better. Although an equivalent number of secondary electrons might be produced as a result of the specimen primary beam interaction, only those that can reach the detector will contribute to the ultimate image. Secondary electrons that are prevented from reaching the detector will generate shadows or be darker in contrast than those regions that have an unobstructed electron path to the detector. It is apparent in the diagram that topography also affects the zone of secondary electron emission. When the specimen surface is perpendicular to the beam, the zone from which secondary electrons are emitted is smaller than found when the surface is tilted. Figure 1.5 illustrates the effect of specimen topography and the position of detector on the secondary electron signals.

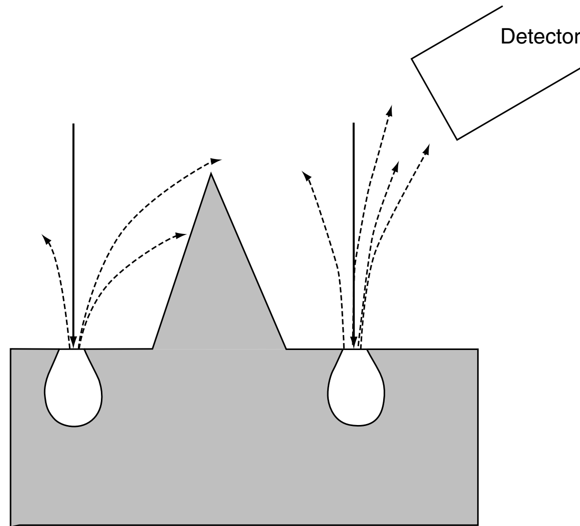

FIGURE 1.5. Illustration of effect of surface topography and position of detector on the secondary electron detection.

Low voltage incident electrons will generate secondary electrons from the very surface region, which will reveal more detailed structure information on the sample surface. More about this will be discussed in Chapter 4.

1.1.3. Backscattered Electrons

Another valuable method of producing an image in SEM is by the detection of BSEs, which provide both compositional and topographic information in the SEM. A BSE is defined as one which has undergone a single or multiple scattering events and which escapes from the surface with an energy greater than 50 eV. The elastic collision between an electron and the specimen atomic nucleus causes the electron to bounce back with wide-angle directional change. Roughly 10–50% of the beam electrons are backscattered toward their source, and on an average these electrons retain 60–80% of their initial energy. Elements with higher atomic numbers have more positive charges on the nucleus, and as a result, more electrons are backscattered, causing the resulting backscattered signal to be higher. Thus, the backscattered yield, defined as the percentage of incident electrons that are reemitted by the sample, is dependent upon the atomic number of the sample, providing atomic number contrast in the SEM images. For example, the BSE yield is ~6% for a light element such as carbon, whereas it is ~50% for a heavier element such as tungsten or gold. Due to the fact that BSEs have a large energy, which prevents them from being absorbed by the sample, the region of the specimen from which BSEs are produced is considerably larger than it is for secondary electrons. For this reason the lateral resolution of a BSE image is

considerably worse (1.0 μm) than it is for a secondary electron image (10 nm). But with a fairly large width of escape depth, BSEs carry information about features that are deep beneath the surface. In examining relatively flat samples, BSEs can be used to produce a topographical image that differs from that produced by secondary electrons, because some BSEs are blocked by regions of the specimen that secondary electrons might be drawn around.

The detector for BSEs differs from that used for secondary electrons in that a biased Faraday cage is not employed to attract the electrons. In fact the Faraday cage is often biased negatively to repel any secondary electrons from reaching the detector. Only those electrons that travel in a straight path from the specimen to the detector go toward forming the backscattered image. Figure 1.6 shows images of Ni/Au heterostructure nanorods. The contrast differences in the image produced by using secondary electron signal are difficult to interpret (Fig. 1.6a), but contrast difference constructed by the BSE signal are easily discriminated (Fig. 1.6b).

The newly developed electron backscattered diffraction (EBSD) technique is able to determine crystal structure of various samples, including nanosized crystals. The details will be discussed in Chapter 2.

1.1.4. Characteristic X-rays

Another class of signals produced by the interaction of the primary electron beam with the specimen is characteristic x-rays. The analysis of characteristic x-rays to provide chemical information is the most widely used microanalytical technique in the SEM. When an inner shell electron is displaced by collision with a primary electron, an outer shell electron may fall into the inner shell to reestablish the proper charge balance in its orbitals following an ionization event. Thus, by the emission of an x-ray photon, the ionized atom returns to ground state. In addition to the characteristic x-ray peaks, a continuous background is generated through the deceleration of high-energy electrons as they interact with the electron cloud

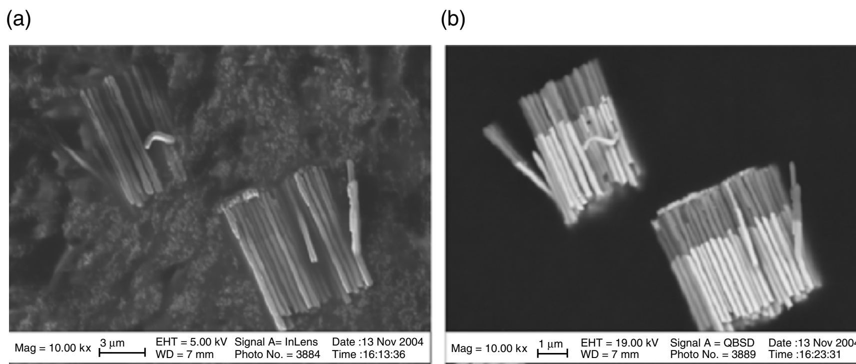

FIGURE 1.6. Ni/Au nanorods images formed by (a) secondary electron signal and (b) backscattering electron signal.

and with the nuclei of atoms in the sample. This component is referred to as the *Bremsstrahlung or Continuum* x-ray signal. This constitutes a background noise, and is usually stripped from the spectrum before analysis although it contains information that is essential to the proper understanding and quantification of the emitted spectrum. More about characteristic x-rays for nanostructure analysis will be discussed in Chapter 3.

1.1.5. Other Electrons

In addition to the most commonly used signals including BSEs, secondary electrons, and characteristic x-rays, there are several other kinds of signals generated during the specimen electron beam interaction, which could be used for microstructure analysis. They are Auger electrons, cathodoluminescence-transmitted electrons and specimen (or absorbed) current.

1.1.5.1. Auger Electrons

Auger electrons are produced following the ionization of an atom by the incident electron beam and the falling back of an outer shell electron to fill an inner shell vacancy. The excess energy released by this process may be carried away by an Auger electron. This electron has a characteristic energy and can therefore be used to provide chemical information. Because of their low energies, Auger electrons are emitted only from near the surface. They have escape depths of only a few nanometers and are principally used in surface analysis.

1.1.5.2. Cathodoluminescence

Cathodoluminescence is another mechanism for energy stabilization following beam specimen interaction. Certain materials will release excess energy in the form of photons with infrared, visible, or ultraviolet wavelengths when electrons recombine to fill holes made by the collision of the primary beam with the specimen. These photons can be detected and counted by using a light pipe and photomultiplier similar to the ones utilized by the secondary electron detector. The best possible image resolution using this approach is estimated at about 50 nm.

1.1.5.3. Transmitted Electrons

Transmitted electrons is another method that can be used in the SEM to create an image if the specimen is thin enough for primary beam electrons to pass through (usually less than 1 μ). As with the secondary and BSE detectors, the transmitted electron detector is comprised of scintillator, light pipe (or guide), and a photomultiplier, but it is positioned facing the underside of the specimen (perpendicular to the optical axis of the microscope). This technique allows SEM to examine the internal ultrastructure of thin specimens. Coupled with x-ray microanalysis, transmitted electrons can be used to acquisition of elemental information and distribution. The integration of scanning electron beam with a transmission electron microscopy detector generates scanning transmission electron microscopy, which will be discussed in Chapter 6.

1.1.5.4. Specimen Current

Specimen current is defined as the difference between the primary beam current and the total emissive current (backscattered, secondary, and Auger electrons). Specimens that have stronger emission currents thus will have weaker specimen currents and vice versa. One advantage of specimen current imaging is that the sample is its own detector. There is thus no problem in imaging in this mode with the specimen as close as is desired to the lens.

2. Configuration of Scanning Electron Microscopes

In this section, we will present a detailed discussion of the major components in an SEM. Figure 1.7 shows a column structure of a conventional SEM. The electron gun, which is on the top of the column, produces the electrons and accelerates them to an energy level of 0.1–30 keV. The diameter of electron beam produced by hairpin tungsten gun is too large to form a high-resolution image. So, electromagnetic lenses and apertures are used to focus and define the electron beam and to form a small focused electron spot on the specimen. This process demagnifies the size of the electron source (~50 μm for a tungsten filament) down to the final required spot size (1–100 nm). A high-vacuum environment, which allows electron travel without scattering by the air, is needed. The specimen stage, electron beam scanning coils, signal detection, and processing system provide real-time observation and image recording of the specimen surface.

2.1. Electron Guns

Modern SEM systems require that the electron gun produces a stable electron beam with high current, small spot size, adjustable energy, and small energy dispersion. Several types of electron guns are used in SEM system and the qualities of electrons beam they produced vary considerably. The first SEM systems generally used tungsten "hairpin" or lanthanum hexaboride (LaB_6) cathodes, but for the modern SEMs, the trend is to use field emission sources, which provide enhanced current and lower energy dispersion. Emitter lifetime is another important consideration for selection of electron sources.

2.1.1. Tungsten Electron Guns

Tungsten electron guns have been used for more than 70 years, and their reliability and low cost encourage their use in many applications, especially for low magnification imaging and x-ray microanalysis [3]. The most widely used electron gun is composed of three parts: a V-shaped hairpin tungsten filament (the cathode), a Wehnelt cylinder, and an anode, as shown in Fig. 1.8. The tungsten filament is about 100 μm in diameter. The V-shaped filament is heated to a temperature of

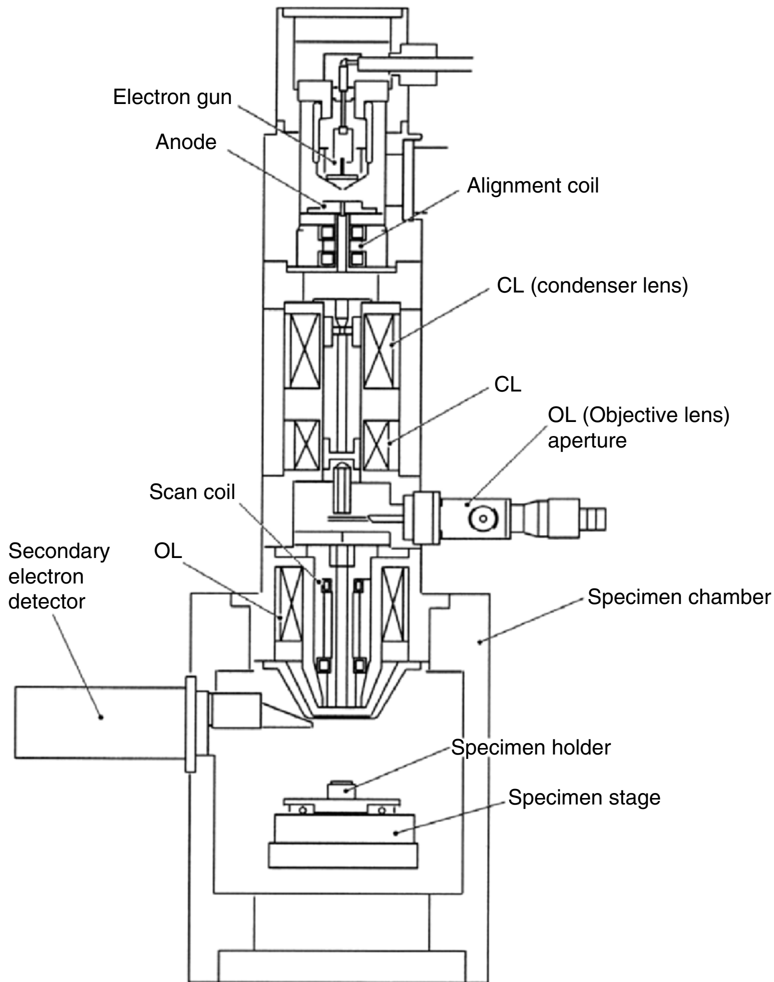

FIGURE 1.7. Schematic diagram of a scanning electron microscope (JSM—5410, courtesy of JEOL, USA).

more than 2,800 K by applying a filament current i_f so that the electrons can escape from the surface of the filament tip. A negative potential, which is varied in the range of 0.1–30 kV, is applied on the tungsten and Wehnelt cylinder by a high voltage supply. As the anode is grounded, the electric field between the filament and the anode plate extracts and accelerates the electrons toward the anode. In thermionic emission, the electrons have widely spread trajectories from the filament tip. A slightly negative potential between the Wehnelt cylinder and the filament, referred to "bias," provides steeply curved equipotentials near the aperture of the

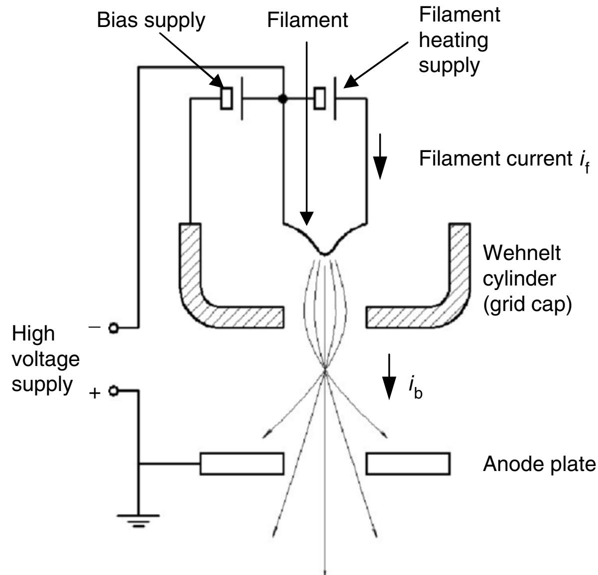

FIGURE 1.8. Schematic of the self-biased thermionic tungsten electron gun. (The effect of the negative bias of the Wehnelt cylinder on the electron trajectory is shown.)

Wehnelt cylinder, which produces a crude focusing of electron beam. The focusing effect of Wehnelt cylinder on the electron beam is depicted in Fig. 1.8.

The electron emission increases with the filament current. There is some “saturation point” of filament current, at which we have most effective electron emission (i.e., the highest electron emission is obtained by least amount of current). At saturation electrons are only emitted from the tip of the filament and focused into a tight bundle by the negative accelerating voltage. If the filament current increases further, the electron emission only increases slightly (Fig. 1.9). It is worth mentioning that there is a peak (known as “false peak”) in beam current not associated with saturation, and this character is different from instrument to instrument, even from filament to another. This false peak is sometimes even greater than the saturation point. Its cause remains unexplained because it is of little practical use, but its presence could be the result of gun geometries during filament heating and the electrostatic creation of the gun’s crossover. Setting the filament to work at the false peak will result in extremely long filament life, but it also deteriorates the stability of the beam. Overheating the filament with current higher than saturation current will reduce the filament life significantly. The burnt-out filament is shown in Fig. 1.10. The spherical melted end of the broken filament due to the overheating is obvious. The filament life is also influenced by the vacuum status and cleanliness of the gun.

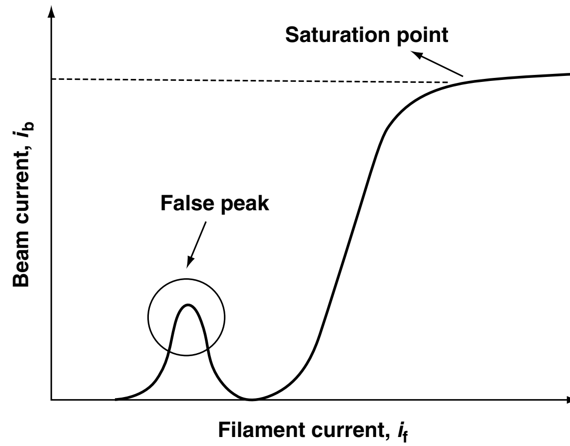

FIGURE 1.9. Saturation of a tungsten hairpin electron gun. At saturation point, majority of the electrons are emitted from the tip of the filament and form a tight bundle by accelerating voltage.

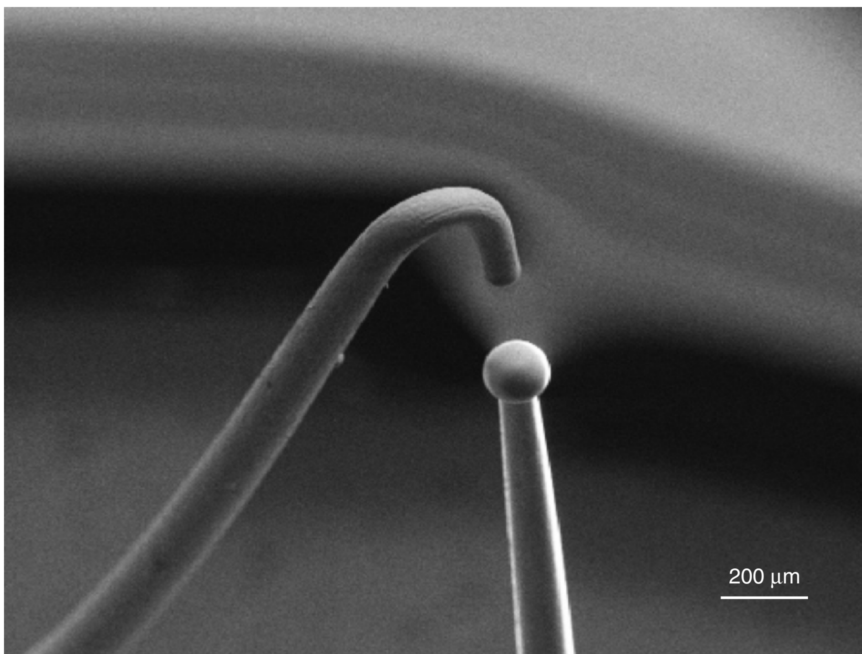

FIGURE 1.10. An SEM image of a "blown-out" tungsten filament due to overheating. A spherical melted end is obvious at the broken filament.

2.1.2. Lanthanum Hexaboride Guns

An alternative for tungsten filament is the LaB_6 filament. This material has a lower work function (2.4 eV) than tungsten (4.5 eV). This means LaB_6 can provide stronger emission of electrons at the same heating temperature. Therefore, LaB_6 electron guns provide 5 to 10× greater brightness and a longer lifetime compared with conventional tungsten guns [4]. Figure 1.11a shows the emitter of a LaB_6 single crystal 100–200 μm in diameter and 0.5 mm long. The crystal is mounted on a graphite or rhenium support, which does not chemically react with the LaB_6 and also serves as the resistive heater to elevate the temperature of crystal so that it can emit electrons. There are several advantages for the use of LaB_6 electron guns. The effective emission area is much smaller than conventional tungsten electron guns, which reduces the spot size of the electron beam. In addition, the electron beam produced by LaB_6 electron guns have smaller energy spread, which means a smaller chromatic aberration and higher resolution of SEM images.

LaB_6 electron source can replace the tungsten electron guns directly in conventional SEMs. However, LaB_6 is readily oxidized at elevated temperatures and the vacuum in gun chamber of conventional electron microscopes is not high enough to avoid contamination on LaB_6 cathode. This reduces the lifetime of the guns significantly. Figure 1.11b shows the details of a used LaB_6 crystal, several contamination spots are easily recognized on its surface. To avoid this situation the chamber electron gun must have a vacuum better than 10^{-8} Torr. Generally, differential pumping of the gun region is needed.

2.1.3. Field Emission Guns

Thermionic sources depend on a high temperature to overcome the work function of the metal so that the electrons can escape from the cathode. Though they are

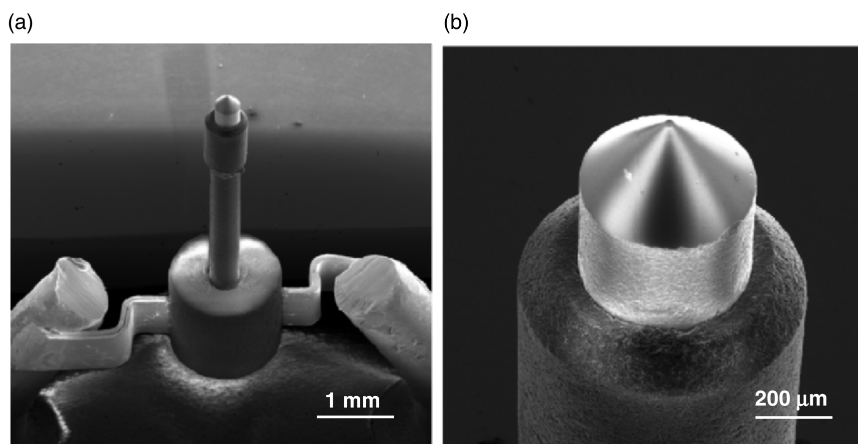

Figure 1.11. (a) SEM image of LaB_6 electron gun and (b) a higher magnification image, small contamination spots are easily recognized.

inexpensive and the requirement of vacuum is relatively low, the disadvantages, such as short lifetime, low brightness, and large energy spread, restrict their applications. For modern electron microscopes, field emission electron guns (FEG) are a good alternative for thermionic electron guns.

In the FEG, a single crystal tungsten wire with very sharp tip, generally prepared by electrolytic etching, is used as the electron source. Figure 1.12a and b shows a micrograph of a typical field emission tip and the schematic structure of the FEG. In this system, a strong electric field forms on the finely oriented tip, and the electrons are drawn toward the anodes instead of being boiled up by the filament heating. Two anodes are used in field emission system, depicted in Fig. 1.12c. The voltage V_1 with a few kilovolts between the tip and the first anode is used to extract the electrons from the tip, and the V_0 is the accelerating voltage.

There are three types of FEGs that are used in the SEM systems [5]. One is the cold field emission (CFE) sources. The "cold field" means the electron sources operate at room temperature. The emission of electrons from the CFE purely depends on the electric field applied between the anodes and the cathode. Although the current of emitted electron beams is very small, a high brightness can still be achieved because of the small electron beam diameter and emission area. An operation known as "flashing" in which the field emission tip is heated to a temperature of more than 2,000 K for a few seconds is needed to clean absorbed gas on the tip. The second class is thermal field emission (TFE) sources, which is operated in elevated temperature. The elevated temperature reduces the absorption of gas molecules and stabilizes the emission of electron beam even when a degraded vacuum occurs. Beside CFE and TFE sources, Schottky emitters (SE) sources are also used in modern SEM system. The performances of SE and CFE sources are superior to thermionic sources in the case of brightness, source size, and lifetime. However, SE source is preferred over CFE source because of its higher stability and easier operation. Because the emitting area of SE source is about 100× larger than that of the CFE source, it is capable to deliver more than 50× higher emission current than CFE at a similar energy spread. Further, a larger size of emission source reduces the susceptibility to vibration.

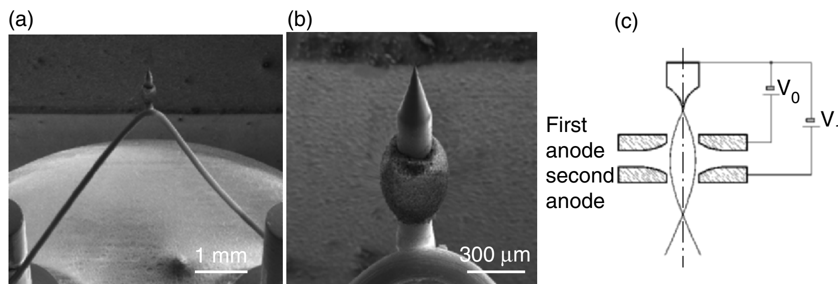

FIGURE 1.12. (a) Field emission source with extreme sharp tip; (b) a higher magnification image; and (c) schematic diagram of a typical field emission electron source. The two anodes work as an electrostatic lens to form electron beams.

Also, electron beam nanolithography needs high emission current to perform a pattern writing, which will be discussed in Chapter 5.

Compared with thermionic sources, CFE provides enhanced electron brightness, typically 100× greater than that for a typical tungsten source. It also possesses very low electron energy spread of 0.3 eV, which reduces the chromatic aberration significantly, and can form a probe smaller than 2 nm, which provides much higher resolution for SEM image. However, field emitters must operate under ultrahigh vacuum (better than 10^{-9} Torr) to stabilize the electron emission and to prevent contamination.

2.2. Electron Lenses

Electron beams can be focused by electrostatic or magnetic field. But electron beam controlled by magnetic field has smaller aberration, so only magnetic field is employed in SEM system. Coils of wire, known as "electromagnets," are used to produce magnetic field, and the trajectories of the electrons can be adjusted by the current applied on these coils. Even using the magnetic field to focus the electron beam, electromagnetic lenses still work poorly compared with the glass lenses in terms of aberrations. The electron lenses can be used to magnify or demagnify the electron beam diameter, because their strength is variable, which results in a variable focal length. SEM always uses the electron lenses to demagnify the "image" of the emission source so that a narrow probe can be formed on the surface of the specimen.

2.2.1. Condenser Lenses

The electron beam will diverge after passing through the anode plate from the emission source. By using the condenser lens, the electron beam is converged and collimated into a relatively parallel stream. A magnetic lens generally consists of two rotationally symmetric iron pole pieces in which there is a copper winding providing magnetic field. There is a hole in the center of pole pieces that allows the electron beam to pass through. A lens-gap separates the two pole pieces, at which the magnetic field affects (focuses) the electron beam. The position of the focal point can be controlled by adjusting the condenser lens current. A condenser aperture, generally, is associated with the condenser lens, and the focal point of the electron beam is above the aperture (Fig. 1.13). As appropriate aperture size is chosen, many of the inhomogeneous and scattered electrons are excluded. For modern electron microscopes, a second condenser lens is often used to provide additional control on the electron beam.

2.2.2. Objective Lenses

The electron beam will diverge below the condenser aperture. Objective lenses are used to focus the electron beam into a probe point at the specimen surface and to supply further demagnification. An appropriate choice of lens demagnification

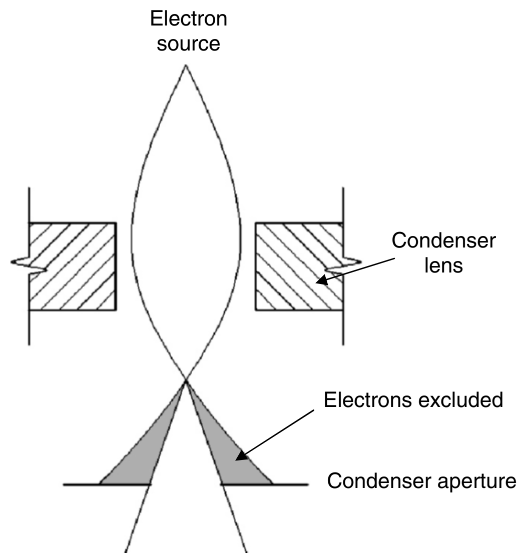

FIGURE 1.13. A diagram showing how the electrons travel through the condenser lens and condenser aperture. Many of the nonhomogeneous or scattered electrons are excluded by the condenser aperture.

and aperture size results in a reduction of the diameter of electron beam on the specimen surface (spot size), and enhances the image resolution.

Three designs of objective lenses are shown in Fig. 1.14 [5]. The asymmetric pinhole lens (Fig. 1.14a) is the most common objective lens. There is only a small bore on the pole piece, and this keeps the magnetic field within the lens and provides a field-free region above the specimen for detecting the secondary electrons. However, this configuration has a large lens aberration. For the symmetric immersion lens (Fig. 1.14b), the specimen is placed inside the lens, which can reduce the focal length significantly. This configuration provides a lowest lens aberration because lens aberration directly scale with the focal length. But the specimen size cannot exceed 5 mm. The Snorkel lens (Fig. 1.14c) produces a strong magnetic field that extends to the specimen. This kind of lens possesses the advantages of the pinhole lens and the immersion lens, combining low lens aberration with permission of large specimen. Furthermore, this configuration can accommodate two secondary electron detectors (the conventional and in-lens detector). The detail detector configurations will be discussed later.

2.3. Column Parameters

It is easy to imagine that spot size and the beam convergence angle α directly relate to the resolution and the depth of focus of the SEM images, but they are influenced by many other parameters such as electron beam energy, lenses

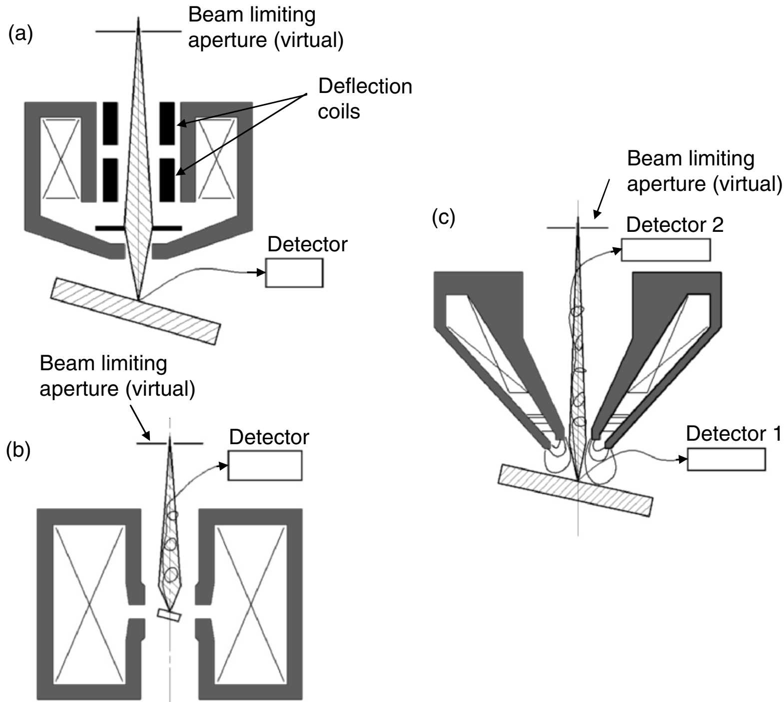

FIGURE 1.14. Objective lens configurations: (a) asymmetric pinhole lens, which has large lens aberration; (b) symmetric immersion lens, in which small specimen can be observed with small lens aberration; and (c) snorkel lens, where the magnetic field extends to the specimen providing small lens aberration on large specimen (Adapted from [5]).

current, aperture size, working distance (WD), and chromatic and achromatic aberration of electron lenses. In this section, several primary parameters that are significant for the image quality will be discussed and a good understanding of all these parameters is needed because these parameters are interdependent.

2.3.1. Aperture

One or more apertures are employed in the column according to different designs of SEM. Apertures are used to exclude scattered electrons and are used to control the spherical aberrations in the final lens. There are two types of aperture: one is at the base of final lens and is known as real aperture; the other type is known as virtual aperture and it is placed in the electron beam at a point above the final lens. The beam shape and the beam edge sharpness are affected by the real aperture. The virtual aperture, which limits the electron beam, is found to have the same affect. The real aperture is the conventional type of aperture system and the virtual aperture is found on most modern SEM system. Because the virtual

aperture is far away from the specimen chamber it can be kept clean for a long time, but the aperture alignment becomes a regular operation, as its size is very small. Decreasing the aperture size will reduce the beam angle α for the same WD, resulting in an enhancement of the depth of field (shown in Fig. 1.15) and a decrease of the current in the final probe. Figure 1.16 shows the electron micrograph of branched grown ZnO nanorods taken with different aperture size. Increase of depth of field due to change of aperture size is easily observed, which is emphasized by circles. An optimum choice of aperture size can also minimize the detrimental effects of aberrations on the probe size [6].

2.3.2. Stigmation

The lens defects (machining errors and asymmetry in lens winding), and contamination on aperture or column can cause the cross section of the electron beam profile to vary in shape. Generally, an elliptical cross section is formed instead of a circular one. As a result during operation, the image will stretch along different direction at underfocus and overfocus condition. This imperfection on the electromagnetic lens is called astigmatism. A series of coils surrounding the electron beam, referred to as "stigmator," can be used to correct astigmatism and achieve an image with higher resolution.

Figure 1.17a shows an SEM image with extreme astigmatism. When moving through focus the image stretches first in one direction (Fig. 1.17b) and when the image is in the in-focus position the stretch is minimized (Fig. 1.17a) before it is stretched to another direction (Fig. 1.17c). The astigmatism correction cycle

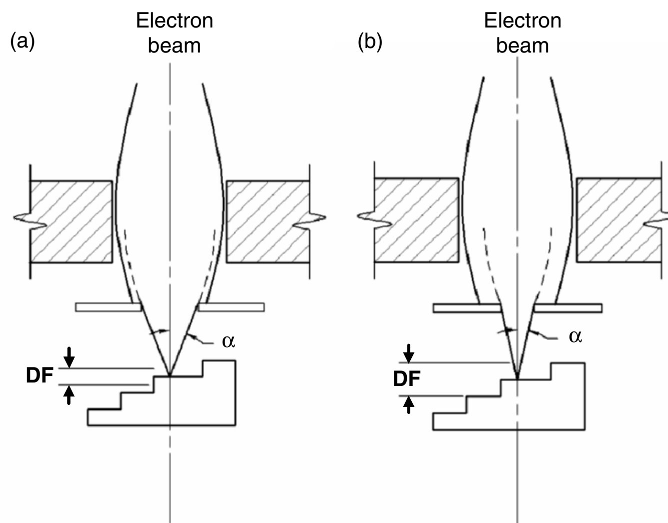

FIGURE 1.15. Small aperture (b) provides enhanced depth of field compared with large aperture (a).